

Received September 28, 2019, accepted October 15, 2019, date of publication October 22, 2019, date of current version November 1, 2019.

Digital Object Identifier 10.1109/ACCESS.2019.2948826

# Improved Dynamic Optimization of PSPF-Based Sources Estimation in Local Multi-Modal Radiation Field

WEIDONG WANG<sup>1</sup>, WENRUI GAO<sup>1</sup>, HONGBIAO ZHU<sup>1</sup>, DONGMEI WU<sup>1</sup>, GUOFU HUANG<sup>2</sup>, AND ZHIJIANG DU<sup>1</sup>, (Member, IEEE)

<sup>1</sup>State Key Laboratory of Robotics and System, Harbin Institute of Technology, Harbin 150001, China

<sup>2</sup>Zhejiang Province Environmental Radiation Monitoring Center, Hangzhou 310000, China

Corresponding author: Zhijiang Du (duzj01@hit.edu.cn)

This work was supported in part by the NSFC under Grant 61773141, and in part by the Natural Science Foundation of Heilongjiang Province under Grant F2018016.

**ABSTRACT** This paper presents a novel Gaussian Processes - Peak Suppression Particle Filter (GP-PSPF) method with adaptive weighting corrections, so as to identify sources in the multi-modal radiation field under some tough conditions, e.g. spatially sparse measurements and sources with large strength differences. As the radiation cumulative effect and ambiguous source number, most existing methods fail to localize the hotspots clustered in narrow regions, and PSPF scheme overcomes these difficulties through multi-layer structure and peak-suppressed correction. In contrast to our earlier work, the proposed algorithm mainly focuses on more severe and practicable conditions, as well as accuracy and robustness improvement. Firstly measurement biases are adopted as the correction feedback through Gaussian Processes technique, and then strength deviation for each particle can be inferred and utilized in two dynamic modules. The dynamic peak-suppressed correction is implemented to achieve more accurate estimations, while the location correction focuses on the solution of location dilemmas, consisting of redundant source identification and less swarm clustering. In addition, scaling adaptation policy and sequential swarm reordering are specially conceived and developed for more stable and accurate optimization. Finally, extensive simulations and physical experiment are conducted under above-mentioned intractable situations, validating the accuracy improvement and practical effectiveness of the algorithm.

**INDEX TERMS** Multiple sources localization, particle filter, multi-modal radiation field, dynamic weighting correction, Gaussian processes.

## I. INTRODUCTION

Owing to the irreversible damage of ionizing radiation to human body, autonomous robots have gradually become substitutions for intervention tasks in facility decommission and nuclear accidents [1]–[4]. Among these intervention demands, a promising topic is efficient environment inspection and rapid localization for radioactive materials [5], [6], but the identification of multi-modal radiation field has not been further investigated and resolved. More specifically, Unmanned Ground Vehicles (UGVs) need to efficiently recognize radioactive hotspots gathered in a narrow region, without prior knowledge about source number and locations. In addition, the estimation method has to be realized

with sparse measurements and cumulative dose information provided by Geiger-Muller detector. Due to the measurement sparsity and cumulative effect of non-directional radiation sensor, most of the traditional methods [12]–[24] fail to identify the multi-modal radiation field in an efficient and non-parametric manner. In the above context, the proposed GP-PSPF solution has been developed to tackle these difficulties.

Benefitting from short latency, small size and low prices, non-directional radiation detectors possess wider applications than directional types, in aspects of sensor network monitoring and robot exploration missions [7]–[11]. Based on non-directional sensors, various formulations have been studied extensively for the multi-source localization problem [11]–[20]. A commonly utilized method is to establish complex probabilistic models for multiple sources, then

The associate editor coordinating the review of this manuscript and approving it for publication was Xiwang Dong.

Expectation Maximization (EM) or Maximum Likelihood Estimation (MLE) can be employed for parameter optimization [12]–[14]. As referenced in [12], the multi-source likelihood model is established with the joint Poisson density, then the Cramer-Rao Bound (CRB) criterion follows to select models with different source number. This method is validated for a circular sensor network, but fails to work when the source number is more than four sources. A similar Bayesian Information Criterion (BIC) is used in Gaussian mixture models to facilitate the determination of radiation source number [13]. Although the cumulative effects are taken into account in above models, the number of radiation sources must be defined in advance, and a lot of time has been wasted in the model selection process. In [15], the cost non-convex models are optimized by gradient decent method, assuming that sources are located in the convex hull of sensor positions. In [16], the search space is discretized and the multiple sources are supposed to locate in finite grids, then source parameters are bundled into sparse matrixes and convex optimization is employed. Unfortunately, these Bayesian estimation methods couldn't be implemented when more than four sources exist, due to the scalable limitation of MLE optimization, i.e., the curse of dimensionality.

Apart from the MLE approaches, stochastic processes are also adopted to approximate the contaminated field [11], [17], [18]. Reggente and Lilienthal [17] take wind information into the gas source identification, by incorporating bivariate Gaussian kernel into the prediction model. This action significantly improves the algorithm feasibility and accuracy of concentration distribution. In [11], Poisson Processes is adopted to combine decentralized Poisson observation of each sensor with centralized decision making of the fusion center, where prediction efficiency of sensor network is enhanced. Beyond the field mapping, Ye *et al.* [18] apply the Gaussian Processes into the strap-down inertial navigation system (SINS), whereby the residual between ground truth and estimated values can be learned to feedback final results. The residual regression idea is quite similar to our proposed method, and achieves robustness and high-precision in the SINS. However, above stochastic methods are only available in cases where few hyper-parameters are involved, and they fail to handle the multi-variable optimization problem without certain source number.

As referenced in [19]–[23], the multi-source identification problem can also be completed through the strength mapping procedure. In literature [19] and [20], exploring region is directly divided into a large quantity of grid cells, and dense sampling is carried out for individual grid. Then the mapping methods are proceeded by data aggregation and spatial correlation techniques, e.g., Gaussian Processes and kernel functions. In contrast to the exhaustive approach, Han and Chen [21] proposes a topological trajectory for source seeking and contour mapping, where both spiral and square paths are applied. A similar method is presented by Newaz *et al.* [22], multiple sources can be identified by aid of contour mapping and variational inference technique.

However, this method depends heavily on the contour lines which may be blurred in mixed radiation field [23]. Another interesting category of algorithms is realized on the basis of particle filter [24], [25], which exists deficiency that multi-modality couldn't be maintained consistently for the inherent unimodality of particle filter [26]. To mitigate the unimodal property, Chin *et al.* [25] introduces the fusion range and mean-shift technique [27] to complete multi-source identification in the surveillance area, but essential issues remain unsolved and sources in close proximity still couldn't be localized. Gao *et al.* [28] develops a PSPF algorithm to tackle the mutual impact of multiple sources. By introducing sequential particle swarms and peak-suppressed weights, non-parametric estimation and multi-modality maintenance can be ensured at the same time. The only shortcoming is that algorithm may fail under some tough conditions [24], e.g. the sources with large strength differences and location mismatching under sparse measurements.

Motivated by above discussions, the GP-PSPF framework intends to implement dynamic weighting corrections and accuracy improvement for severe conditions, as well as excellent scalability for multivariable optimization. The advantages of proposed algorithm are listed as follows.

i) Instead of the direct regression, anisotropy Gaussian Processes is employed to obtain bias information about vehicle-based measurements after each iteration. Contrary to other model-based fitting methods [29], this non-parametric regression can not only realize variable-scale fitting, but also show noisy robustness with the Gaussian assumption.

ii) Dynamic strength and location corrections are constructed to correct particle weights through strength deviation surface. The strength factor mainly affects particle weighting through the peak-suppression module, providing sufficient strength range for optimization, while the location factor accelerates swarm movement in position aspect. By aid of two dynamic treatments some intractable conditions can be overcome, and confidence improvement obtained.

iii) Due to the drastic state changes in estimation process, scaling adaptive policy is developed to allocate effective phases for both dynamic modules. That is, the location factor plays a role in the transition stage, while the strength module is mainly useful for strength accuracy improvement, resulting into more efficient and stable procedure.

iv) Coupled with the sequential swarm structure, an extra reordering mechanism is conceived to resort particle swarm by centroid strength. This treatment can alleviate the dilemma that redundant sources are identified without destroying algorithm foundation, i.e., strength suppression mechanism and sequential swarm structure.

The remaining of article is organized as follows: section II mainly describes the studied issues and corresponding preliminaries such as PSPF algorithm and Gaussian Processes method. In section III, several major components of the GP-PSPF algorithm are expounded and clarified, as well as overall flow chart and pseudo-code provided. Then various simulations and field experiment coupled with quantitative

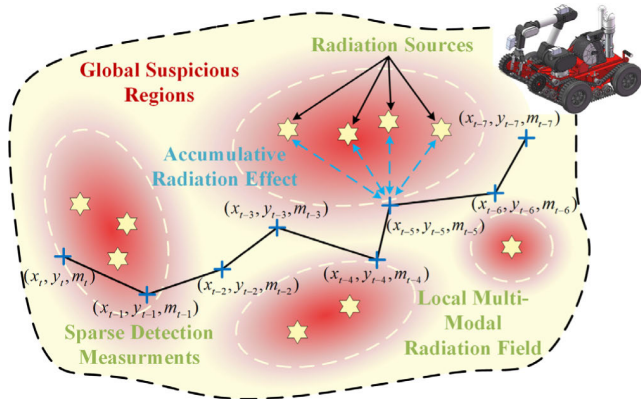


FIGURE 1. The scenario of vehicle-base exploration and accumulative effect of radiation detector.

analysis are completed in section IV, to verify effectiveness of the proposed algorithm under intractable scenarios. Finally, section V concludes the paper and future research is prospected.

## II. PROBLEM STATEMENT AND PRELIMINARIES

### A. PROBLEM STATEMENT

Our research focuses on how to exactly identify the multiple radiation sources from local multimodal field, under spatially sparse measurements with accumulative radiation effect. In many practical applications [24], global hazardous region is indeed consist of several local multimodal radiation fields, while each local region possesses radiation sources with uncertain number. The unmanned robot equipped with GM counter is utilized to inspect the suspicious region and deliver intensity measurements back to operation terminal, as shown in Fig. 1. Considering the vehicle mobility requirement and sluggish detection response [1], collected measurements for multi-modality field are always spatially sparse. Furthermore, the principle that GM sensors perceive radiation intensity by calculating ionizing flux leads to the fact that only noisy cumulative intensity is available, which aggravates the difficulty of local multi-source estimation.

In the multimodal radiation environment, the source information can be represented by two-dimensional location and a scalar intensity, i.e.,  $A_j = \{A_j^x, A_j^y, A_j^{str}\}$ , for  $1 \leq j \leq K$ . Additionally, the gamma-ray complies with inverse square propagation in the air and exponential decay in objects [30], thus the multimodal strength distribution can be formulated with these effective source parameters. For a specific sensing location  $S_i$ , the spatial strength for individual source component and cumulative detection model can be respectively calculated in the following equations.

$$\mathcal{I}(S_i, A_j) = \frac{A_j^{str}}{h^2 + |S_i - A_j^{pos}|^2} \exp\left(\sum_{b \in (\mathcal{B} \cap \overline{S_i A_j})} -\mu_b l_b\right) \quad (1)$$

$$I(S_i, \mathcal{A}) = E_i \cdot \sum_{j=1}^K \mathcal{I}(S_i, A_j) + B_i \quad (2)$$

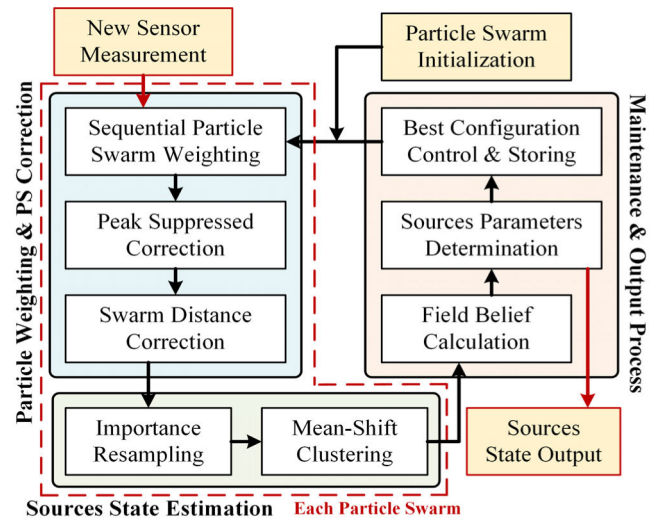


FIGURE 2. Overall flowchart of the PSPF algorithm.

where  $h$  indicates the height difference from sensing plane to radiation source, and  $\mu_b$  and  $l_b$  are the decay coefficient and obstacle thickness respectively. In (2),  $E_i$  denotes the conversion constant from  $nGy/h$  to CPS (counts per second), and  $B_i$  represents the background radiation component under stochastic volatility, generally ranging from 50 to 200  $nGy/h$  in nuclear-free environment.

In our earlier research, the PSPF framework has successfully tackled multiple sources maintenance and non-parametric estimation problems in the multimodal radiation field [28]. However, the algorithm solution still has defects under some practicable conditions, i.e., the radiation sources with large strength differences, location mismatching under sparse measurements and redundant source identification as the peak-suppressed correction, as described in section 2.2.

This paper attempts to take fully advantage of regression information about deviated measurements, and dynamically adjust particle weights in particle strengths and estimated locations respectively. Through these dynamic adaptation links, the modified PSPF scheme can enhance not only speed and accuracy, but also algorithm robustness, i.e., prediction errors like source dislocation and fake identification can be significantly avoided. Since the regression procedure relies on Gaussian Processes, this dynamically improved framework is called GP-PSPF in our paper.

### B. PSPF ALGORITHM

In the specific case of locally coupled radiation field, the PSPF solution mainly overcomes the challenges of inherent algorithmic defects and detector limitations, consisting of: i) accumulative radiation effect, ii) spatially sparse measurements, iii) ambiguous prior on sources number [13], iv) inherent unimodal performance of particle filter [26]. The overall flow chart of PSPF is illustrated in Fig. 2, which can be divided into: i) particle weighting and correction, ii) sources estimation for sequential particle swarms, iii) configuration

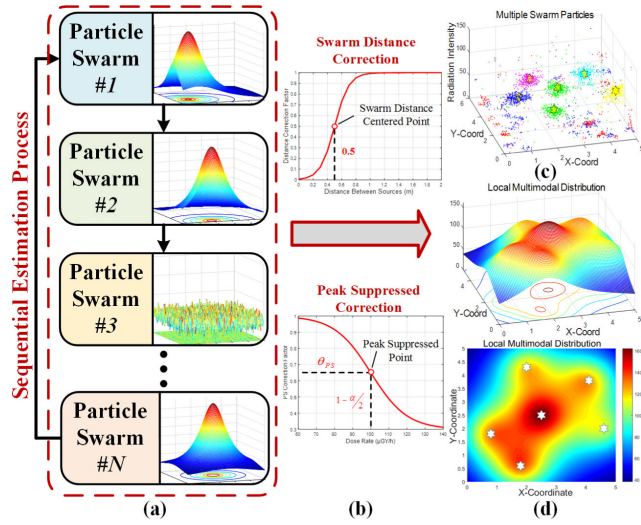


**FIGURE 3.** The prediction structure with multi-layer particle swarms and working mechanism. (a) Sequential estimation process. (b) Weighting correction mechanism. (c) The predicted status of each swarm. (d) Actual multimodal distribution and identified results.

maintenance and determination. For a better understanding of efforts and innovations in this paper, it's essential to explain the implementation techniques of PSPF mathematically, as introduced in the following.

### 1) MULTI-LAYER PARTICLE SWARMS STRUCTURE

To achieve the capability of stable optimization and multi-source estimation, PSPF algorithm separates the unified state space into multiple particle swarms, and each particle swarm is responsible for estimating individual radiation sources. Meanwhile, these particle swarms are integrated as a sequential structure in the observation weighting process, as shown in Fig. 3(a). Assume that candidate centroids of particle swarms are represented as  $\{C_s\}_{s=1}^{M_s}$ , and  $\mathcal{P}_s = \{p_{r,s} \in \mathbb{R}^3 | r = 1, \dots, M_r\}$  denotes the particle states of the  $s$ -st particle swarm, for  $s = 1, \dots, M_s$ . Thus the observation weight for each particle  $p_{r,s}$  can be calculated, accompanied with actual detection measurements  $m(S_i)$  and other swarm centroids  $C_{-s}$ , as expressed in (3).

$$w_{obs}(m(S_i), p_{r,s}, C_{-s}) = \frac{poi(m(S_i) | I'(p_{r,s}, C_{-s}))}{poi(\lfloor I'(p_{r,s}, C_{-s}) \rfloor | I'(p_{r,s}, C_{-s}))} \quad (3)$$

where  $I'(\cdot)$  denotes the cumulative radiation model [shown in (2)] with multiple estimated centroids  $C_{-s}$  and  $p_{r,s}$ , and  $\lfloor \cdot \rfloor$  depicts the floor operator. Additionally, the function  $poi(\cdot)$  represents the Poisson observation model, whereby actual count  $k$  is regarded as total dose measurements  $m(S_i)$  and expected count  $\lambda$  denotes the estimated result in current iteration, as shown in (4).

$$poi(X = k | \lambda) = \frac{\lambda^k e^{-\lambda}}{k!} \quad (4)$$

Sequential estimation structure can not only get rid of the dilemma that cumulative measurements couldn't be directly applied to Poisson observation model, but also realize non-parametric estimation about radiation source number, i.e., redundant particle swarm would be randomly distributed in the estimation space when there exists no redundant strength. This non-parametric and implicit setting has been shown in Fig. 3(a). Furthermore, it has been verified that processing runtime of PSPF is linear to pre-defined swarm number, avoiding the exponential complexity and dimension disaster, as referenced in [28].

### 2) PARTICLE WEIGHT CORRECTION

Besides the multi-layer swarms structure, two sigmoid-like correction factor has also been incorporated into the particle weighting process, as shown in Fig. 3(b). That is, peak suppressed correction is adopted to decrease the particle weights with larger strength, while swarm distance correction can avoid meaningless position substitution between particle swarms. The functions of corrected factors can be seen in (5) and (6), whereby  $\theta_{dist}$  and  $\theta_{ps}$  denote the offset value of sigmoid functions,  $b_{dist}$  and  $b_{ps}$  are the scale parameters respectively, and  $\alpha$  indicates the vertical tuning parameter of peak-suppressed function.

$$w_{dist}(p_{r,s}, C_{-s}) = \frac{1}{1 + \exp[\frac{\theta_{dist} - dist(p_{r,s}, C_{-s})}{b_{dist}}]} \quad (5)$$

$$w_{ps}(p_{r,s}, \theta_{ps}) = (1 - \alpha) + \alpha \cdot \frac{1}{1 + \exp[(p_{r,s}^{str} - \theta_{ps})/b_{ps}]} \quad (6)$$

Assisted with these correction measures, the modified state space can effectively inhibit inherent unimodal property of particle filter, and achieve excellent performance about stable iteration and non-parametric estimation. The predicted results can be seen in Fig. 3(c) and 3(d), and the synthesized weight is calculated by (7).

$$w_{syn}(p_{r,s}, C_s, m(S_i)) = w_{ps}(p_{r,s}, \theta_{ps}) \cdot w_{dist}(p_{r,s}, C_{-s}) \cdot w_{obs}(p_{r,s}, C_s, m(S_i)) \quad (7)$$

It should be noted that the suppressed center  $\theta_{ps}$  plays an important role in robust prediction and multimodal maintenance. In our earlier work, this parameter is fixed to 90% of the maximum measurement through empirical testing. In the proposed scheme, a dynamic adjustment strategy is created and tested, to acquire performance improvement in prediction speed, practicability and robustness.

### 3) SOURCES STATE ESTIMATION AND STATE MAINTENANCE MECHANISM

As indicated in Fig. 2, sequential importance sampling and state estimation are carried out with the weighting step. To determine whether candidate centroid exists in each swarm, mean-shift clustering and filtering criterion are applied in the estimation module. The mean-shift technique is actually an iterative optimization procedure [27], where particle density and shift vector are estimated with specific kernel

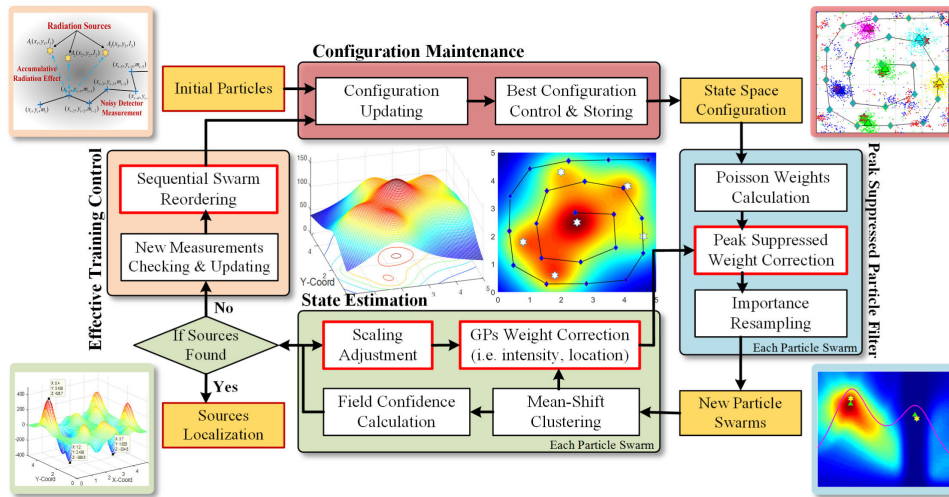


FIGURE 4. Flow chart of the improved GP-PSPF algorithm.

functions. The calculation of state shift  $M(x)$  is expressed in (8), whereby Gaussian kernel  $\phi_H(x)$  and synthesized particle weight  $w(p_i)$  are applied in our PSPF solution.

$$\begin{cases} M(x) = \frac{\sum_{\mathcal{P}} w(p_i) \cdot \phi_H(p_i - x) \cdot (p_i - x)}{\sum_{\mathcal{P}} w(p_i) \cdot \phi_H(p_i - x)} \\ \phi_H(x) = (2\pi)^{-3/2} |H|^{-1/2} \exp(-\frac{1}{2} x^T H^{-1} x) \end{cases} \quad (8)$$

where  $H$  is the diagonal matrix with scale parameters, and  $x$  represents three-value centroid in current iteration. After the mean-shift procedure, the filtering criteria of percent threshold  $THR_{pr}$  and intensity threshold  $THR_{str}$  is applied in each swarm layer, determining whether the centroid of biggest identified cluster is a valid estimate.

In addition to above two measures, the last important part in PSPF algorithm is the configuration maintenance module, responsible for recording and restoring particle states with highest confidence score. With assistance of the protection mechanism, previous estimation procedure can avoid being wasted under the risk of multi-layer structure collapse. In the maintenance module, the average observation weight of all sensor measurements can be regarded as the evaluation function, as expressed in (9).

$$\mathcal{F} = \frac{1}{N} \sum_{i=1}^N w_{obs}(m(S_i), C_s) = \frac{1}{N} \sum_{i=1}^N \frac{p(m(S_i) | I'(S_i, C_s))}{p(I'(S_i, C_s) | I'(S_i, C_s))} \quad (9)$$

### C. GAUSSIAN PROCESSES REGRESSION

Gaussian processes is a widely applied and powerful nonlinear regression approach [31]. Instead of specifying intrinsic structure assumptions as prior (e.g. the degree of a polynomial), this method utilizes kernel machine and standard training procedure to achieve a fairly reliable black-box model, while the inference process completed in a quite simple and principled way. The regression procedure can be divided

into parameter training and data prediction. That is, hyper-parameters can be obtained firstly by maximizing the log-evidence function  $\log p(y|X, \theta)$ , then tested states  $x_*$  can be inferred under Gaussian assumption. The formulation about predicted probability  $p(x_*|X, y, \theta)$  can be expressed in the following.

$$\begin{cases} \mu_* = m(x_*) + k(x_*, x)(K(x, x) + \sigma_n^2 I)^{-1}(y - m(x)) \\ \sigma_*^2 = k(x_*, x_*) - k(x_*, x)(K(x, x) + \sigma_n^2 I)^{-1}k(x, x_*) \end{cases} \quad (10)$$

where  $k(\cdot, \cdot)$  and  $K(\cdot, \cdot)$  respectively denote vector and matrix constructed by kernel function,  $\mu_*$  and  $\sigma_*^2$  represent the predicted mean and variance of the posteriori  $p(x_*|X, y, \theta)$ , and  $\sigma_n^2$  is the Gaussian noise variance.

In the GP-PSPF algorithm, Gaussian Processes regression is adopted to obtain the deviation surface between actual measurements and predicted intensity, then the regression surface can provide adaptive compensation information in both location and intensity aspects, of which is expounded in section 3.2 and section 3.3.

## III. DESIGN AND ANALYSIS OF GP-PSPF ALGORITHM

### A. OVERALL GP-PSPF FRAMEWORK

This section mainly describes the overall framework and dynamic correction mechanism of the GP-PSPF algorithm, with spatially sparse measurements collected in the cross-mixed radiation environment. In the proposed method, strength deviation surface is firstly obtained through Gaussian Processes technique [29], then these deviation messages are integrated into the weight correction process in both aspects of location and strength. That is, the peak-suppressed offset and location correction factor for each particle can be dynamically adjusted by the strength deviation priori. Through these varying correction modules, more accurate and robust results can be obtained in the multi-source estimation scheme, as well as rapidity performance achieved.

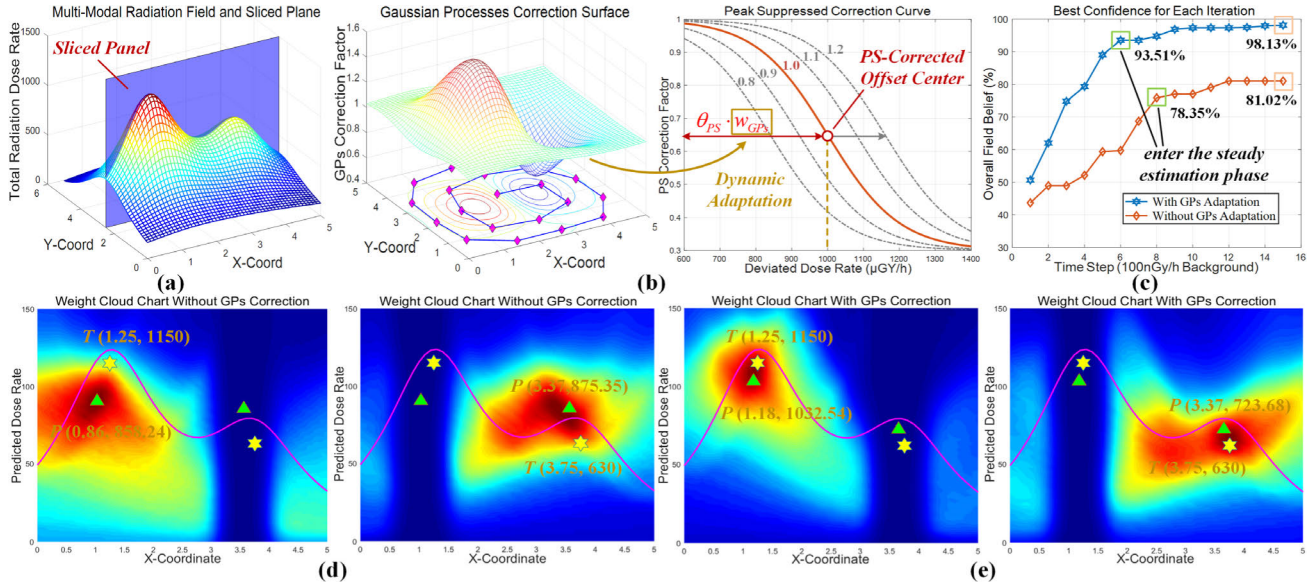


**FIGURE 5. The working mechanism and performance of GPs-based strength correction. (a) Multimodality field. (b) Deviation surface and adaptive correction center. (c) Confidence results. (d) Fixed scheme without GP correction. (e) Dynamic scheme with GP correction.**

As expounded above, the GP-based weighting modules are incorporated into the GP-PSPF scheme to address the following problems: i) the co-existence of radiation sources with large strength differences; ii) location mismatching and redundant source identification under extreme sparse measurements; iii) less swarm clustering for the cancellation effect among multiple sources.

### B. GAUSSIAN PROCESSES CORRECTION ON SOURCE STRENGTH

In our previous paper, an empirical and unified value is adopted for the peak-suppression module [28]. Although the sigmoid function allows optimized shifts in a certain range [Fig.3 (b)], the fixed correction manner may not work well in some specific conditions. Enlightened by the idea that particle weights in different locations should be suppressed with different values, strength deviation information is adopted to regulate peak-suppressed offsets in different positions, motivating particle swarms towards actual source states, as shown in Fig. 5(b). Similar to definitions in section 2.2,  $\{m(S_i)\}_{i=1}^N$  and  $\{I(S_i, C_s)\}_{i=1}^N$  respectively denote actual measurements and predicted dose intensity at location  $S_i$ , then deviated strength dataset  $D$  can be constructed according to (11), whereby symbol definitions are similar to previous equations.

$$D = \{x_i, y_i | x_i = S_i, y_i = m(S_i) - I(S_i, C_s)\}_{i=1}^N \quad (11)$$

Depending on above deviation measurements, Gaussian Processes is utilized to regress deviation surface and calculate correction factor in different positions. The implementation details of Gaussian Processes have been introduced in

section 2.3, while sigmoid function<sup>1</sup> is adopted to adapt the peak-suppressed offset, as expressed in (12).

$$\left\{ \begin{array}{l} \text{prediction :} \\ y_* = m(x_*) + k(x_*, x)(K(x, x) + \sigma_n^2 I)^{-1}(y - m(x)) \\ \text{calculation :} \\ w_{IntGPs} = \frac{2}{1 + \exp[-y_*/(b_{Int} \cdot b_{IntConf})]} \end{array} \right. \quad (12)$$

where  $b_{Int}$  represents the scale parameter for correction squashing function, and  $b_{IntConf}$  is the regulation parameter associated with overall field confidence, as explained in section 3.4. Following the regression step, strength correction module with varying suppressed center is employed to pursue more accurate estimation procedure, as expressed in (13), which is similar to traditional PSPF solution [shown in (6)] but a dynamic factor  $w_{IntGPs}$  is newly added into the correction procedure.

$$w_{ps}(p_{r,s}, w_{IntGPs}) = (1 - \alpha) + \alpha \cdot \frac{1}{1 + \exp[(p_{r,s}^{str} - \theta_{ps} \cdot w_{IntGPs})/b_{ps}]} \quad (13)$$

To clarify the positive effect of dynamic strength correction on peak-suppression module, simple simulations and mechanism analysis have been conducted under both dynamic and static conditions. As illustrated in Fig. 5(a), two sources with large strength differences are located in the same vertical plane, i.e., (1.25, 2.5, 1150) and (3.75, 2.5, 630). Instead of

<sup>1</sup>Other squash functions with S-Shape, e.g. Turkey's bi-weight and tanh function, are also available and useful, but sigmoid-like functions are adopted to keep consistent with the GPs classification method [32].

unified and empirical suppression, the strength deviation surface is utilized to feedback suppression center in the dynamic model, that is, suppressed level should be increased if strength deviation is positive and vice versa, as shown in Fig. 5(b). The confidence scores under both conditions are compared in Fig. 5(c), and it can be observed that strength correction model performs much better than the static version, reaching to 98.1% and 81.02% respectively. The failure of PSPF method stems from the following reason: the large source-related swarm is over-suppressed by the empirical suppression center, while the mutual effect prevents another swarm from approaching the actual strength of small source in strength dimension.

Weighting distributions of the sliced panel are calculated under different particle states and suppressed models, where Fig. 5(d) shows the cloud chart under steady states of PSPF scheme, and Fig. 5(e) is the dynamic correction method. By comparing weighing distributions and confidence results, it can be summarized as follows: i) although PSPF method can localize two radiation sources, the unified suppression operation results in an unreliable confidence score (78.35%), followed by the dilemma that optimization process is stuck and limited. ii) With assistance of adaptive bias correction, the dynamic prediction model can obtain more accurate estimates in strength aspect. Additionally, the weighting cloud chart and high confidence (93.51%) verify the validation of strength feedback mechanism.

**C. GAUSSIAN PROCESSES CORRECTION ON LOCATIONS**

Besides strength correction module, deviation regression surface is also used in location aspect to facilitate weight differentiation and particle movement, which provide opportunities to solve the issues caused by sparse measurements. Different from the strength correction, the location correction is directly integrated into the synthesized weighting process. Given strength deviation surface, the location-related correction factor for each particle state  $p_{r,s}$  can be calculate through (14).

$$w_{PosGPs}(p_{r,s}, b_{PosConf}) = \frac{2}{1 + \exp[-y_*(p_{r,s}) / (b_{Pos} \cdot b_{PosConf})]} \quad (14)$$

where  $y_*(p_{r,s})$  indicates the strength bias at location  $p_{r,s}$ , and  $b_{Pos}$  and  $b_{PosConf}$  represent empirical scale parameter and adaptive scale factor for the location-related correction function. Assisted with the location correction, several intractable situations, such as location mismatching and redundant or less source identification, can be better solved. For a better explanation of the working mechanism, simulations with three radiation sources and detailed analysis have been performed in the following parts.

**1) LOCATON MISMATCHING UNDER SPARSE MEASUREMENTS**

As illustrated in Fig. 6(a) and 6(b), the particle swarm #1 cannot approach actual left source with the PSPF method,

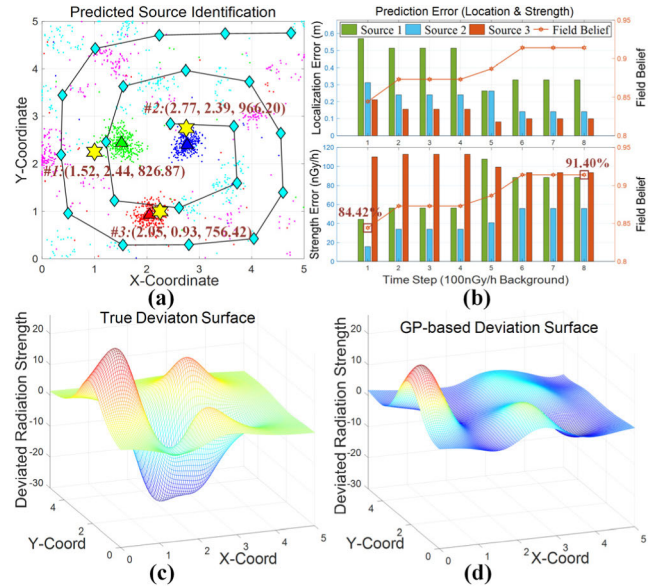


**FIGURE 6. The location mismatching scene for three radiation sources. (a) Initial particle states. (b) Actual strength deviation surface. (c) GP-based deviation surface.**

and the optimization procedure is stuck at an unreliable level (91.40%). Through weighting analysis and observation, we can conclude that the location mismatching is mainly caused by spatially sparse measurements. That is, the estimated centroid and actual source affect equally to the nearby observation, while the weighting difference for other longer-distance measurements is not large enough to migrate particle swarm towards the actual state. In addition, the mutual effect among multi-layer particle swarms also hinders state migration of one single swarm, making the problem more difficult to resolve.

We intend to integrate the location correction measure into particle weighting process to ease particle movement in location aspect. Instead of the strength correction for more accurate estimates, the location module mainly motivates particles towards right locations by enlarging weighting differences. This module also regards the GP-based deviation regression as feedback information, and actual deviation surface and GP-based regression surface are respectively shown in Fig. 6(c) and 6(d). It can be seen that all the major deviations are captured in the regression surface, which is sufficient for location correction despite of the sparse measurements.

To understand the influence of dynamic factors on the location mismatching issue, various univariate simulations are carried out with the same initial states. For the sake of analysis and comparison, simulations in each model are performed 10 times and the statistical results (i.e., location errors and confidence scores) are listed in Fig. 7. In addition, the weighting distributions of particle swarm #1 before and after corrections are also mapped, coupled with different dynamic factors, as shown in Fig. 8. The observations and conclusions are summarized as follows:

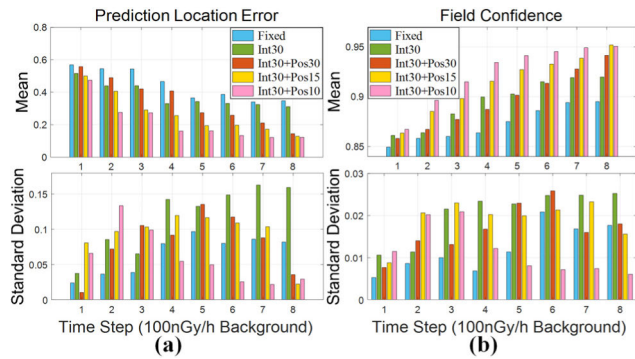


FIGURE 7. Location error and field confidence results under different models. (a) Prediction location error. (b) Results of field confidence.

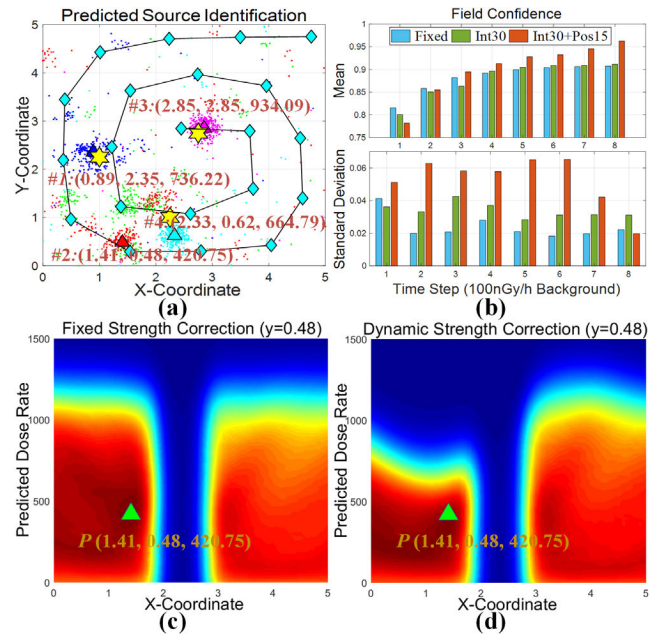


FIGURE 9. The redundant sources identification scene and quantitative analysis. (a) Initial particle states. (b) Field confident results. (c) and (d) shows weighting panels with fixed and dynamic strength model.

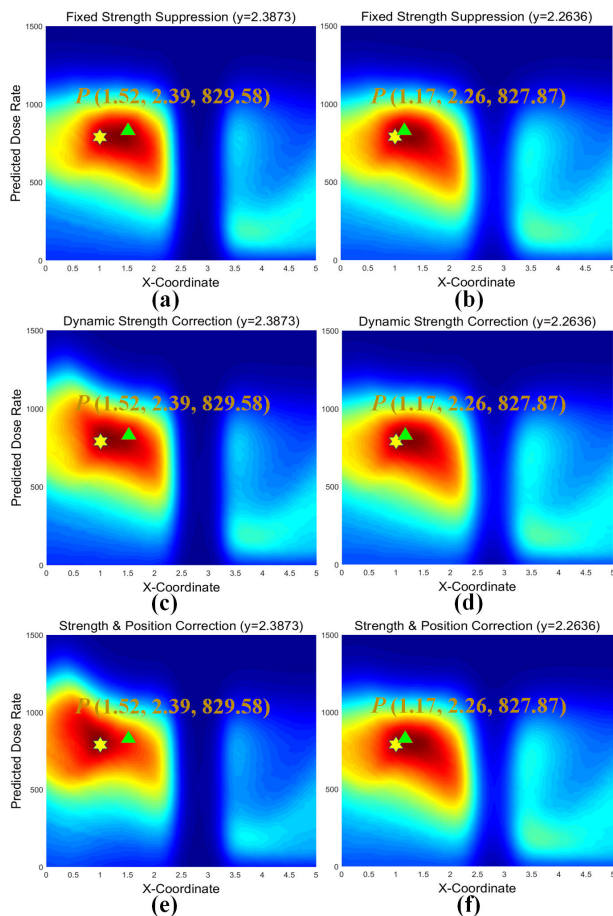


FIGURE 8. Weighting distributions of two estimated states under different models. (a-b) Traditional PSPF model. (c-d) Dynamic strength model. (e-f) Dynamic strength & position model.

i) Although strength correction module (i.e., the Int30 condition in Fig. 7) plays a positive role on the mismatching issue, the improvement is limited (91.96%) in the strength dimension and there exist many prediction failures, which can be inferred from the large variances of location errors and confidences in Fig. 7. In contrast to the strength module, the location correction factor can enhance position movement by enlarging weighting differences, leading to

notable belief improvement and state correction, as shown in Fig. 8(a), 8(c) and 8(e).

ii) By comparing the statistical results under different location scale parameters (i.e., Int30+Pos10: 95.07%, Int30+Pos15: 95.20%, Int30+Pos30: 94.16%), we can see that the model with smaller scale can obtain satisfactory predictions much faster and more easily whilst it is accompanied with greater state changes. That may cause frequent collapse of the multi-layer structure. Consequently, tradeoff between model sensitivity and estimation stability should be balanced when selecting the empirical scale in location correction module.

iii) The weighting distributions of two states before and after the prediction procedure, are respectively calculated with different correction models, as depicted in Fig. 8. By comparing three pre-predicted distributions in Fig. 8(a), 8(c) and 8(e), only the dynamic location model has a significant effect on weighting movement. After the prediction process, location factor plays little effect on weighting correction, while strength factor works well to improve the estimated accuracy, as shown in Fig. 8(b), 8(d) and 8(f). To dispatch both dynamic modules, the scale adaptation policy is conceived and developed in section 3.4.

## 2) REDUNDANT SOURCES IDENTIFICATION AND ERASING MECHANISM

Another intractable situation is the redundant sources identification, caused by the swarm distance factor inherited from the PSPF algorithm. An example is shown in Fig. 9(a). The exclusive effect of distance factor greatly reduces other particle weights around the swarm centroid #2, thus the fake

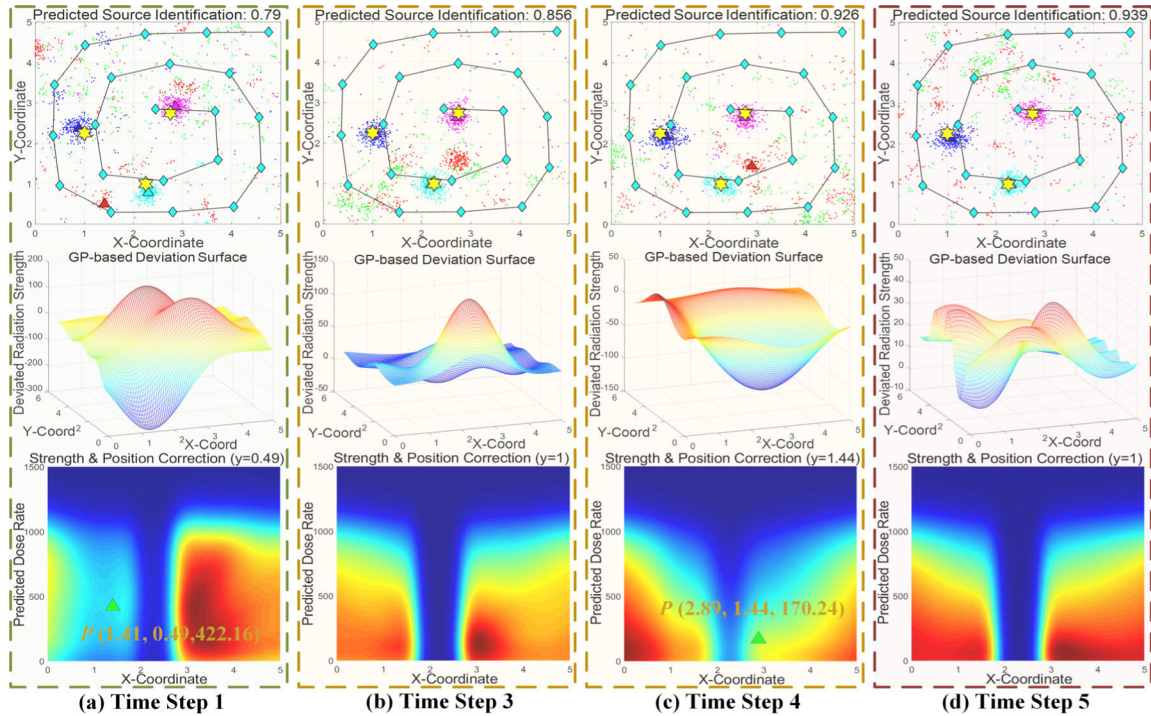


**FIGURE 10.** The prediction procedure of redundant sources identification scene, coupled with deviation regression and weighting distributions. (a-d) represents each step of the prediction procedure, respectively.

source remains clustering status and confidence score stuck in unreliable level, as illustrated in the Fixed and Int30 conditions of Fig. 9(b). Above dilemma is also observed through the weighting distributions shown in Fig. 9(c) and 9(d), both of which could not dispel particle swarm #2 as the peak-suppression module is useless on particle movement.

Coupled with location correction factor, the weights of particle swarm #2 can be significantly reduced due to the large negative bias, resulting into fake source erasing and high confidence. The whole prediction procedure is listed in Fig. 10, where greater state changes and larger confidence variance occurs in the optimization process. This is due to the utilization of both dynamic factors is easy to break the unstable balance between multiple swarms, this conclusion can also be inferred from the large confidence variance in Fig. 9(b). Furthermore, an extra reordering operation is developed to resort swarm order by estimated strength after each iteration. This treatment is helpful to dispel particle states with relative low strength estimates, without abandoning the multi-layer structure and peak-suppression mechanism.

#### D. THE SCALING ADAPTIVE POLICY

In the proposed algorithm, the strength correction mainly focuses on strength accuracy improvement, while the location correction plays a role in state movement in position aspect. That is, the dynamic location factor works in the unsteady and transition stages while the strength factor is in the steady stage, as illustrated in Fig. 11. Enlightened by above facts, a belief-based adaptive policy is conceived to

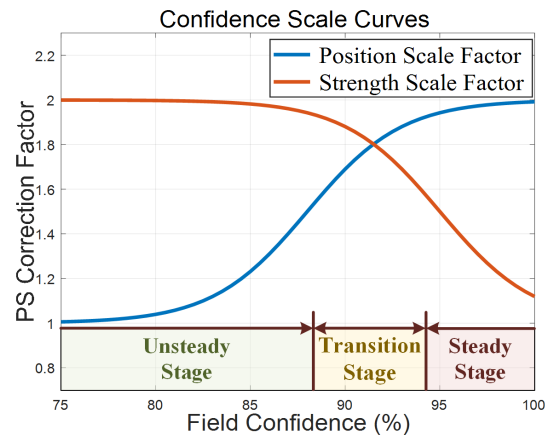


**FIGURE 11.** Confidence scale factors  $b_{IntConf}$  and  $b_{PosConf}$  under different confidences.

allocate effective phases for both correction modules. The adaptive scales  $b_{IntConf}$  and  $b_{PosConf}$  are incorporated into factor calculation in (12) and (14), and the varying factors are defined in (15) and (16).

$$b_{PosConf} = 1 + \frac{1}{1 + \exp[(0.88 - \text{conf})/0.025]} \quad (15)$$

$$b_{IntConf} = 1 + \frac{1}{1 + \exp[(\text{conf} - 0.95)/0.025]} \quad (16)$$

The effect of scaling adaptive module is summarized as follows: i) in unsteady phases, the location module performs to motivate particles towards correct locations, without incurring large variation of peak-suppressed value to ensure

multimodal balance and stable estimation. Thus smaller location scale is employed relative to the strength scale at this time. ii) In steady phases, the source locations have almost been completed, and more attentions are paid on strength accuracy of individual radiation source. The strength scale is set smaller to handle bias information more sensitively, while location scale is larger to alleviate the mutual impact.

### E. THE COMPLETE ALGORITHM SCHEME

As expounded above, the synthesized particle weights can be calculated according to (17), as shown at the bottom of this page where  $w_{PosGP_s}$  and  $w_{IntGP_s}$  respectively denote the dynamic location factor and strength factor, and other definitions are similar to (7).

By incorporating strength deviation priori, location factor and strength factor into the PSPF framework, the proposed algorithm can effectively tackle the intractable situations under sparse measurements and multimodal radiation field. The Pseudo code of the GP-PSPF algorithm is shown in Algorithm 1.

### IV. SIMULATION AND EXPERIMENTAL RESEARCH

In this section, more complex simulations and real-world experiments are completed to verify the practicable effect of the GP-PSPF algorithm. As the linear time-consuming and robustness performance have been previously validated in the PSPF framework [28], the experimental research mainly focuses on the factors and effects associated with dynamic correction modules, i.e., source relocation by the position factor, accuracy improvement by the strength factor and extra time consumption by the regression process, etc. It is noteworthy that the spiral trajectories utilized in simulations are derived from real-world experiment to facilitate result comparison. Table 1 lists the scenario setting and parameters in simulations and field experiment.

#### A. SIMULATION 1: LOCATION MISMATCHING WITH A LARGE NUMBER OF SOURCES

The location mismatching scenario for 6 radiation sources is illustrated in Fig. 12(a): since the cumulative strengths generated by particle swarms #1, #2 and #3 nearly compensate for measurements in the left region, extra particle swarms couldn't cluster and identify source in the middle region. We attempt to explain the reasons why particles couldn't cluster in the area with apparent strength deviation [Fig. 12(b)], and detailed weighting analysis is performed under different corrected conditions, consisting of fixed correction, location correction, strength correction, strength & position correction. Each case has been repeated for 10 times and the average field confidence can be seen in Fig. 12(c). The simulation results are analyzed as follows:

#### Algorithm 1 Pseudo Code for GP-PSPF Estimation Scheme

**Inputs:** sequential radiation measurements  $\mathcal{I} = \{I_n\}_{n=1}^N$ , consisting of total dose rate and corresponding locations.

**Outputs:** estimated radiation sources  $\mathcal{A} = \{A_k\}_{k=1}^K$ , each centroid is a three-value vector similar to input state.

- 1 **Particle Swarm Initialization:** randomly sampling a three-value vector from state space, for each particle  $p_{r,s}$ .
- 2 **for** each sequential measurement  $I_n$  ( $n = 1, \dots, N$ ) **do**
- 3     Resort particle swarm  $\{C_{s,n}\}_{s=1}^{M_s}$  in descending order by centroid strength.
- 5     Regress strength bias set  $D$  with Gaussian Processes technique, and compute scale factors  $b_{IntConf}$  and  $b_{PosConf}$  if  $\mathcal{F}$  is beyond  $THR_{GP}$  (as shown in (15) and (16)).
- 6     **for** each particle swarm  $\mathcal{P}_s$  ( $s = 1, \dots, M_s$ ) **do**
- 7         **for** each particle state  $p_{r,s}$  ( $r = 1, \dots, M_r$ ) **do**
- 8             Calculate dynamic correction factors  $w_{IntGP_s}$  and  $w_{PosGP_s}$  with (12) and (14), then synthesized particle weight  $w_{syn}^{s,r}$  can be obtained by (3), (5) and (13).
- 9         **end for**
- 10         Resample the  $s$ -st swarm with synthesized weights and obtain new particle swarm  $\{p_{s,r}^n\}_{r=1}^{M_r}$ .
- 11         Determine whether or not particle swarm has a cluster centroid with the mean-shift method (as shown in (8)).
- 12         **end for**
- 13         Calculate the field confidence  $\mathcal{F}$  according to (9), then determine whether to update best configuration or recover previous one.
- 14     **end for**
- 15 **Output** estimated states if  $\mathcal{F}$  is beyond  $THR_{pr\_end}$ .

i) Through the weighting calculation on plane  $y=2.5$  [Fig. 12(d-f)], it can be found that high-weight states only concentrate under the strength & position model, but are widely dispersed in the low-strength region under fixed and dynamic location conditions. This phenomenon verifies the effectiveness of the location correction, which strengthens the weighting differences in position aspect.

ii) Although apparent strength deviation exists in the middle region, the sparse detection points and relatively low strength bias are the reasons for the non-clustering dilemma. Without location correction module, the particle states are impossible to cluster just through random optimization, and all other promotion measures become useless. In this perspective, the dynamic location correction provides foundation for sustained optimization.

$$w_{syn}(p_{r,s}, C_s, m(S_i)) = w_{PosGP_s}(p_{r,s}, b_{PosConf}) \cdot w_{ps}(p_{r,s}, w_{IntGP_s}) \cdot w_{dist}(p_{r,s}, C_{-s}) \cdot w_{obs}(p_{r,s}, C_s, m(S_i)) \quad (17)$$

**TABLE 1. Parameter settings in different simulations and experiments.**

Scenario Item	Parameter Setting
• Size of Surveillance area	5 m × 5 m
• Trajectory of measurements	Spiral-shape trajectory (from real-world experiment)
• Number of particles in each swarm	350
• Particle swarm number	8
• Radiation source number	6
Scene #1	(0.8,1.8,680), (1.8,0.6,820), (4.6,2,565), (4.1,3.8,720), (2,4,3,670), (2,5,2,5,870)
• Concerned condition	Location mismatching
• Particle swarm number	8
• Radiation source number	5
Scene #2	(0.5,1.7,655), (1.8,0.5,730), (4,2,3,630), (2,2,4,2,670), (2,5,2,5,870)
• Concerned condition	Less swarm clustering
• Particle swarm number	8/8/5
• Radiation source number	6/5/3
• Parameters about source	Similar to above conditions
• Concerned condition	Processing runtime
• Particle swarm number	4
• Radiation source number	2
Field experiment	(1.5,2.5,11370), (2,2.5,7380) (by handheld detector)
• Parameters about source	Sources with large strength differences
• Concerned condition	

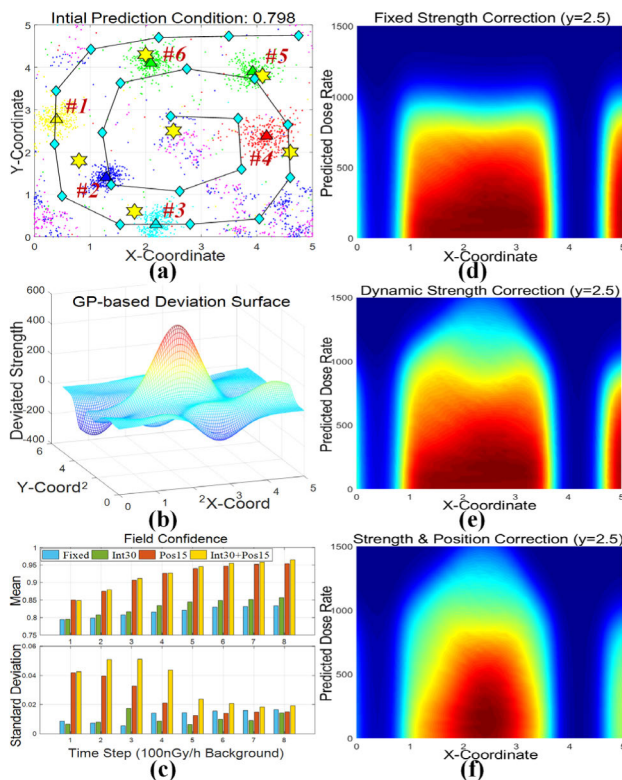


**FIGURE 12. The complex location mismatching and weighting analysis.**

iii) Fig. 12(c) illustrates the confidence scores under four correction models, the results also indicate that the location module is the critical factor on problem solving. Additionally, the large variances under location & strength model imply

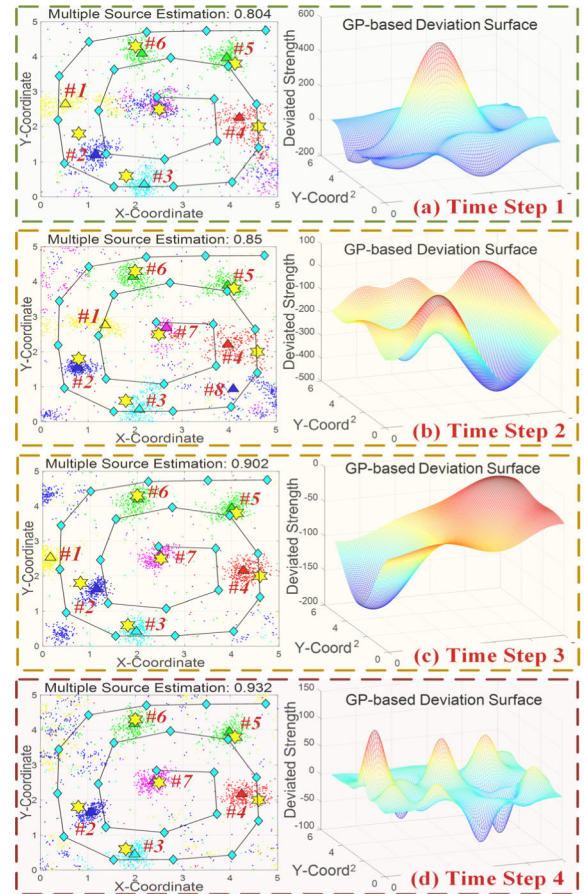


**FIGURE 13. The prediction procedure under strength & position condition.**

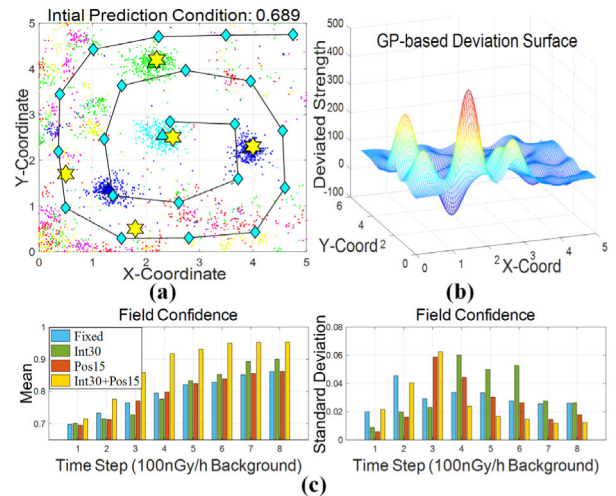


**FIGURE 14. The less swarm clustering scenario for cancellation effect and confidence results.**

the utilization with both factors would result into larger state changes before steady phases, as discussed in section 3.4.

Fig. 13 shows the estimation procedure in the strength & position condition, the particle swarm #7 is firstly clustered in the middle region through the location factor [Fig.13 (a-b)],

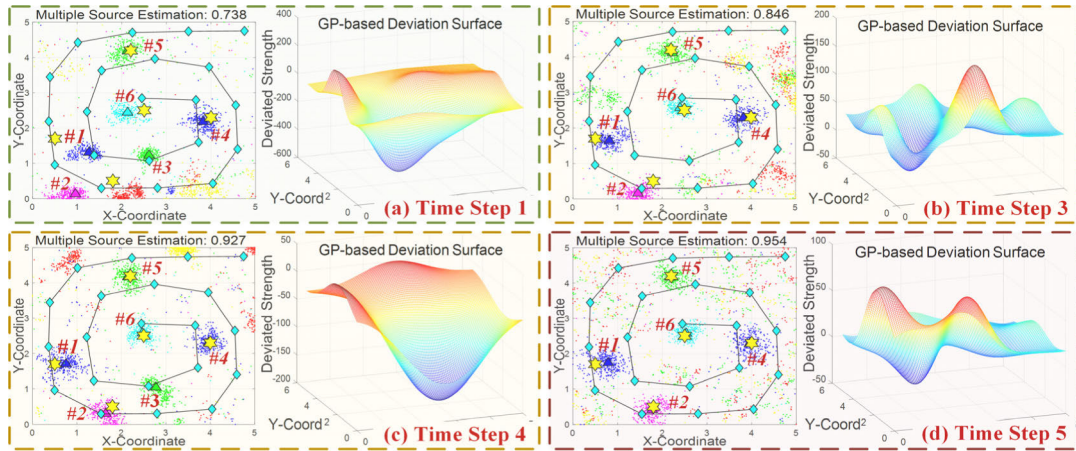


FIGURE 15. The prediction procedure and deviation surface for less swarm clustering situation.

then particle swarm #1 is dispelled as the large negative deviation [Fig.13 (c)], and finally radiation sources are correctly identified and accuracy promotion is realized in strength aspect [Fig.13 (d)]. This simulation combines location factor, strength factor and scaling adaptive technique to successfully tackle the complex location mismatching scenario, validating high efficiency and robustness performance of the proposed algorithm.

**B. SIMULATION 2: LESS SWARM CLUSTERING FOR THE CANCELLATION EFFECT**

The less swarm clustering situation may occur when several small radiation sources are gathered in close proximity. The example is shown in Fig. 14(a), where a single swarm is clustered in the lower-left region between two actual sources. This is a challenging situation as the following reasons: i) once the particle swarm moves towards one actual source, the confidence score would decrease significantly. As the limitation of configuration maintenance, optimal states may not be updated if other swarms could not identify efficiently in several iterations. ii) The peak-suppression module may not work for estimates with low strength, that is, the unimodal preference of particle filter could not be mitigated by the peak-suppression module.

Based on the analysis, both dynamic correction modules are implemented to accelerate particle movement and suppress strength level in an adaptive manner. The confidence results are illustrated in Fig. 14(c), verifying that expected correction effect cannot be achieved by individual location and strength correction modules. That is, strength correction module cannot effectively move the weighted particles, while location module cannot identify extra source in limited iterations. The GP-PSPF method, integrated with both adaptive modules, can handle above two issues at the same time. That is, particles are rapidly motivated by the location factor, and then efficient source identification by strength factor. In addition, the high confidence score and low variance verify

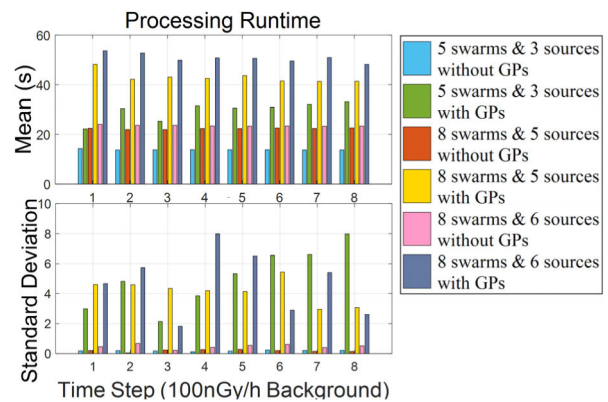


FIGURE 16. The statistical results of processing runtime under deferent conditions (i.e. particle swarms, actual sources and Gaussian correction).

the robustness and accuracy performance of the bi-correction algorithm.

The prediction procedure for the GP-PSPF framework is illustrated in Fig. 15, and the following facts can be observed: drastic state changes and belief fluctuations always occur in initial steps; but once two swarms aggregate in the local region, the confidence score and estimations accuracy would be promoted in a rapid speed.

**C. SIMULATION 3: PROCESSING RUNTIME TEST**

This simulation mainly concerns on the extra effect of Gaussian regression module on source number scalability and running time. As shown in Fig. 16, the simulation is divided into six experimental groups with different swarm number, source number and Gaussian processes modules, and each condition is repeated for 10 times. The algorithm is conducted in the computer with 2.80GHZ Intel Core i5 and 8GB RAM, and average runtime and corresponding variance are presented in Fig. 16.

The statistical results not only verify the linear complexity of multi-layer estimation structure, but also show

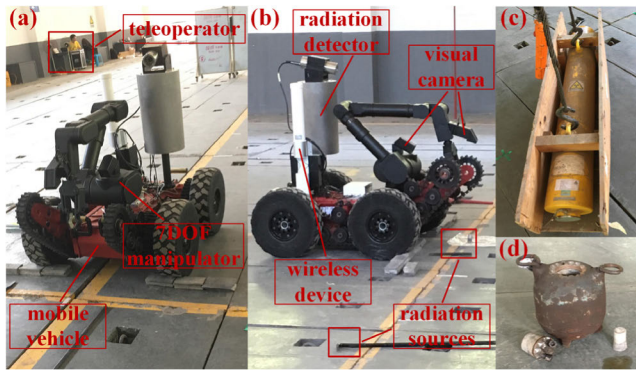


FIGURE 17. The real-world experiment for radiation sources with large strength differences.

the efficiency improvement of dynamic modules, and two conclusions can be drawn: i) In the conditions without GP-based corrections, processing time is roughly linear to the pre-defined swarm number, i.e., 0.656s (5 swarms), 1.063s (8 swarms) and 1.119s (8 swarms) for each sequential iteration. Additionally, the low variances indicate that static models can strictly control time consumption, which is helpful to formulate online exploration strategy. ii) The time consumption significantly increases with dynamic correction models, and average span for each cycle reaches to 1.404s (5 swarms), 2.046s (8 swarms) and 2.417s (8 swarms). Extra consumption comes from the optimization process of GPs parameters, which also causes the large variance in Fig. 16. Although GP regression prolongs the prediction duration, the online property still remains as the time consumptions under all conditions are never more than 60.638s in one cycle.

**D. FIELD EXPERIMENT: RADIATION SOURCES WITH LARGE STRENGTH DIFFERENCES**

The field experiment is conducted for sources with large strength differences to validate the robustness of GP-PSPF algorithm, and the scenario is illustrated in Fig. 17. A mobile robot equipped with GM counter (VACUTAC, 70031) is employed to collect measurements in the surveillance area, while the controlling terminal is deployed far away to avoid radiation injury. Three Co-60 radiation sources are employed in the experiment, as indicated in Fig. 17(b), whereby two sources are gathered together as the large hotspot and the third one placed 2.5m away to be the small hotspot. Both the hotspots have been previously measured by handheld-type detector, i.e., 11570nGy/h and 7380nGy/h at the 1m distance. Additionally, 275nGy/h background dose is adopted in the prediction process.

Besides the GP-based adaptive corrections, two types of exploring trajectories, e.g. spiral shape and lawn shape, are adopted to determine which one is more efficient, as shown in Fig.18. The strength regression by Gaussian Processes is also depicted in Fig.18, indicating that sources could not be identified through sparse measurements and simple regression technique. Both the GP-PSPF estimation and traditional

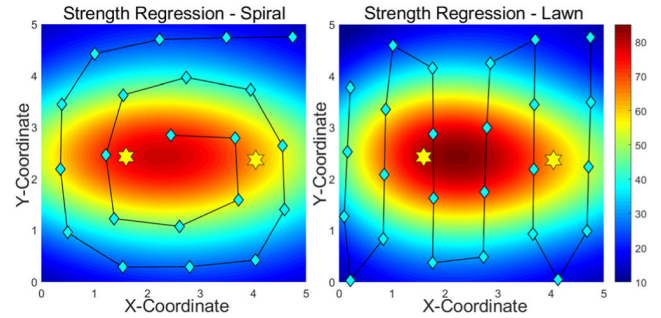


FIGURE 18. Two categories of exploring trajectories and strength distributions with simple GP regression.

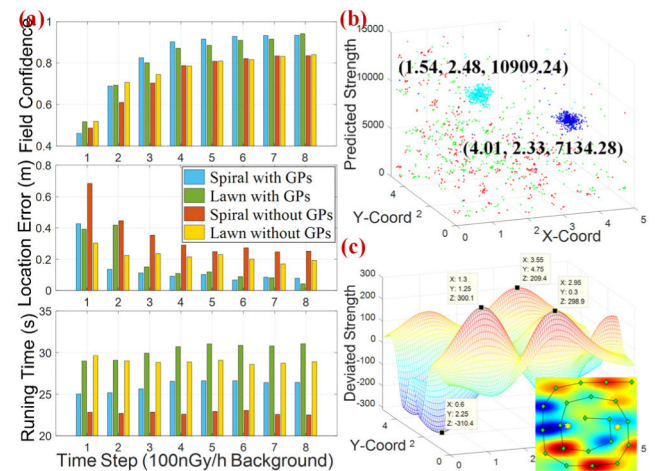


FIGURE 19. Quantitative analysis of field experiment. (a) Prediction results and processing time. (b) Final particle states. (c) Strength deviation regression with spiral-shape measurements.

PSPF are carried out for 5 times and finally quantitative results are listed in Fig.19, we can draw conclusions as follows:

i) In the scenario with large differentiated sources, both algorithms work well in non-parametric estimation about source number, but the GP-PSPF has better accuracy and rapid performance than traditional method, as inferred from confidence and location results.

ii) As the final confidences of spiral and lawn trajectories are nearly the same, i.e., 93.45% and 94.16%, we can conclude that prediction accuracy has little relation with exploring trajectory, but with the detection density. Additionally, the violent fluctuations of strength residual, ranging from -300nGy/h to 310nGy/h, not just verify the robustness of proposed algorithm, but indicate that occlusions may occur when detector is close to radiation sources.

iii) The total runtime of GP-PSPF method are individually 208.4s and 242.5s under spiral and lawn trajectories. Although the processing speed is slower than that of the static model (i.e. 181.4s and 232.1s), the GP-based corrections can significantly improve the optimization efficiency, and moreover, are sufficient for the multi-source estimation problem.

## V. CONCLUSION

In conclusion, a modified PSPF-based scheme with dynamic weighting corrections is proposed to tackle several tough scenarios in multimodal radiation field. Assisted with the Gaussian Processes technique and strength deviation surface, the GP-PSPF algorithm can adapt to the peak-suppressed value in a dynamic manner, achieving more accurate estimates (i.e., strength and location) and higher confidence score. In the location aspect, a similar correction factor is incorporated into the weighting process to handle some intractable situations, consisting of redundant sources identification and less swarm clustering, and whilst the correction mechanisms have been analyzed in detail and verified through simulations. Additionally, scaling adaptation policy and sequential swarm reordering are developed in above dynamic weighting modules, not only remaining the non-parametric property about source number, but also improving accuracy and stability performance. Simulations with large source number and field experiment have been conducted and validated in several aspects, i.e., location mismatching, redundant or less swarm clustering, processing speed, exploration trajectory and non-parametric property. All the experimental results are sufficient to validate the practicability and robustness of the proposed method. Therefore, the GP-PSPF algorithm makes it possible to explore an unknown radiation environment and estimate multi-source states in robust, accurate and non-parametric property. Our future research may focus on trajectory planning and radiation source estimation in an online manner.

## ACKNOWLEDGMENT

(Weidong Wang and Wenrui Gao contributed equally to this work.)

## REFERENCES

- [1] R. R. Murphy, J. Peschel, C. Arnett, and D. Martin, "Projected needs for robot-assisted chemical, biological, radiological, or nuclear (CBRN) incidents," in *Proc. IEEE Int. Symp. Saf., Secur., Rescue Robot. (SSRR)*, Nov. 2012, pp. 1–4.
- [2] F. E. Schneider, J. Welle, D. Wildermuth, and M. Ducke, "Unmanned multi-robot CBRNE reconnaissance with mobile manipulation system description and technical validation," in *Proc. 13th Int. Carpathian Control Conf. (ICCC)*, May 2012, vol. 318, pp. 637–642.
- [3] A. Ruggiero and M. Vos, "Communication challenges in CBRN terrorism crises: Expert perceptions," *J. Contingencies Cris. Manag.*, vol. 23, no. 3, pp. 138–148, Sep. 2015. doi:10.1111/1468-5973.12065.
- [4] C. Ducros, G. Hauser, N. Mahjoubi, P. Girones, L. Boisset, A. Sorin, E. Jonquet, J. M. Falcicola, and A. Benhamou, "RICA: A tracked robot for sampling and radiological characterization in the nuclear field," *J. Field Robot.*, vol. 34, no. 3, pp. 583–599, May 2017. doi:10.1002/rob.21650.
- [5] P. Deusdado, E. Pinto, M. Guedes, F. Marques, P. Rodrigues, A. Lourenço, R. Mendonça, A. Silva, P. Santana, J. Corisco, M. Almeida, L. Portugal, R. Caldeira, J. Barata, and L. M. Flores, "An aerial-ground robotic team for systematic soil and biota sampling in estuarine mudflats," in *Adv. Intell. Syst. Comput.*, vol. 418, pp. 15–26, Nov. 2016. doi:10.1007/978-3-319-27149-1\_2.
- [6] I. Tsitsimpelis, C. J. Taylor, B. Lennox, and M. J. Joyce, "A review of ground-based robotic systems for the characterization of nuclear environments," *Prog. Nucl. Energy*, vol. 111, pp. 109–124, Mar. 2019. doi:10.1016/j.pnucene.2018.10.023.
- [7] H. Ardiny, S. Witwicki, and F. Mondada, "Autonomous exploration for radioactive hotspots localization taking account of sensor limitations," *Sensors*, vol. 19, no. 2, p. 292, Jan. 2019. doi:10.3390/s19020292.
- [8] H. E. Baidoo-Williams, *Novel Techniques for Estimation and Tracking of Radioactive Sources*. Iowa City, IA, USA: University of Iowa, 2014.
- [9] B. Ristic, M. Morelande, and A. Gunatilaka, "Information driven search for point sources of gamma radiation," *Signal Process.*, vol. 90, no. 4, pp. 1225–1239, Apr. 2010. doi:10.1016/j.sigpro.2009.10.006.
- [10] A. F. García-Fernández, L. Svensson, and M. R. Morelande, "Multiple target tracking based on sets of trajectories," *IEEE Trans. Aerosp. Electron. Syst.*, to be published. doi:10.1109/TAES.2019.2921210.
- [11] C. D. Pahlajani, I. Poulakakis, and H. G. Tanner, "Networked decision making for Poisson processes with applications to nuclear detection," *IEEE Trans. Autom. Control*, vol. 59, no. 1, pp. 193–198, Jan. 2014. doi:10.1109/TAC.2013.2267399.
- [12] M. Morelande, B. Ristic, and A. Gunatilaka, "Detection and parameter estimation of multiple radioactive sources," in *Proc. 10th Int. Conf. Inf. Fusion*, Jul. 2007, pp. 1–7.
- [13] W. Ding and X. Cheng, "Fault tolerant target tracking in sensor networks," in *Proc. 10th ACM Int. Symp. Mobile Ad Hoc Netw. Comput.*, May 2009, pp. 125–134.
- [14] C. Q. Wu, M. L. Berry, K. M. Grieme, S. Sen, N. S. V. Rao, R. R. Brooks, and G. Cordone, "Network detection of radiation sources using localization-based approaches," *IEEE Trans. Ind. Informat.*, vol. 15, no. 4, pp. 2308–2320, Apr. 2019. doi:10.1109/TII.2019.2891253.
- [15] H. E. Baidoo-Williams, S. Dasgupta, R. Mudumbai, and E. Bai, "On the gradient descent localization of radioactive sources," *IEEE Signal Process. Lett.*, vol. 20, no. 11, pp. 1046–1049, Nov. 2013. doi:10.1109/LSP.2013.2279499.
- [16] Y. Cheng and T. Singh, "Source term estimation using convex optimization," in *Proc. 11th Int. Conf. Inf. Fusion*, Jun./Jul. 2008, pp. 1–8.
- [17] M. Reggente and A. J. Lilienthal, "Using local wind information for gas distribution mapping in outdoor environments with a mobile robot," in *Proc. IEEE Sensors*, Oct. 2009, pp. 1715–1720. doi:10.1109/ICSENS.2009.5398498.
- [18] W. Ye, J. Li, J. Fang, and X. Yuan, "EGP-CDKF for performance improvement of the SINS/GNSS integrated system," *IEEE Trans. Ind. Electron.*, vol. 65, no. 4, pp. 3601–3609, Apr. 2018. doi:10.1109/TIE.2017.2748048.
- [19] N. Cao, K. H. Low, and J. M. Dolan, "Multi-robot informative path planning for active sensing of environmental phenomena: A tale of two algorithms," in *Proc. Int. Conf. Auton. Agents Multi-Agent Syst. (AAMAS)*, 2013, pp. 7–14.
- [20] C. Q. Wu, M. L. Berry, K. M. Grieme, S. Sen, N. S. V. Rao, R. R. Brooks, and G. Cordone, "A source-attractor approach to network detection of radiation sources," in *Proc. IEEE Int. Conf. Multisensor Fusion Integr. Intell. Syst. (MFI)*, Sep. 2016, pp. 394–399.
- [21] J. Han and Y. Chen, "Multiple UAV formations for cooperative source seeking and contour mapping of a radiative signal field," *J. Intell. Robot. Syst.*, vol. 74, nos. 1–2, pp. 323–332, Apr. 2014. doi:10.1007/s10846-013-9897-4.
- [22] A. A. R. Newaz, S. Jeong, H. Lee, H. Ryu, N. Y. Chong, and M. T. Mason, "Fast radiation mapping and multiple source localization using topographic contour map and incremental density estimation," in *Proc. IEEE Int. Conf. Robot. Autom. (ICRA)*, May 2016, pp. 1515–1521.
- [23] B. Li, Y. Zhu, Z. Wang, C. Li, Z.-R. Peng, and L. Ge, "Use of multi-rotor unmanned aerial vehicles for radioactive source search," *Remote Sens.*, vol. 10, no. 5, p. 728, May 2018. doi:10.3390/rs10050728.
- [24] D. Shah and S. Scherer, "Robust localization of an arbitrary distribution of radioactive sources for aerial inspection," in *Proc. WM Conf.*, Oct. 2017, pp. 1–15.
- [25] J.-C. Chin, D. K. Y. Yau, and N. S. V. Rao, "Efficient and robust localization of multiple radiation sources in complex environments," in *Proc. 31st Int. Conf. Distrib. Comput. Syst.*, Jun. 2011, pp. 780–789.
- [26] J. Vermaak, A. Doucet, and P. Pérez, "Maintaining multimodality through mixture tracking," in *Proc. 9th IEEE Int. Conf. Comput. Vis.*, vol. 2, Oct. 2003, pp. 1110–1116.
- [27] D. Comaniciu and P. Meer, "Mean shift: A robust approach toward feature space analysis," *IEEE Trans. Pattern Anal. Mach. Intell.*, vol. 24, no. 5, pp. 603–619, May 2002. doi:10.1109/34.1000236.
- [28] W. Gao, W. Wang, H. Zhu, G. Huang, D. Wu, and Z. Du, "Robust radiation sources localization based on the peak suppressed particle filter for mixed multi-modal environments," *Sensors*, vol. 18, no. 11, p. 3784, Nov. 2018. doi:10.3390/s18113784.
- [29] S. Filip, A. Javeed, and L. N. Trefethen, "Smooth random functions, random ODEs, and Gaussian processes," *SIAM Rev.*, vol. 61, no. 1, pp. 185–205, Jan. 2019. doi:10.1137/17M1161853.

- [30] C. I. Thompson, E. E. Barritt, and C. Shenton-Taylor, "Predicting the air fluorescence yield of radioactive sources," *Radiat. Meas.*, vol. 88, pp. 48–54, May 2016. doi: [10.1016/j.radmeas.2016.02.013](https://doi.org/10.1016/j.radmeas.2016.02.013).
- [31] S. Ambikasaran, D. Foreman-Mackey, L. Greengard, D. W. Hogg, and M. O'Neil, "Fast direct methods for Gaussian processes," *IEEE Trans. Pattern Anal. Mach. Intell.*, vol. 38, no. 2, pp. 252–265, Feb. 2016. doi: [10.1109/TPAMI.2015.2448083](https://doi.org/10.1109/TPAMI.2015.2448083).
- [32] P. Bergström and O. Edlund, "Robust registration of point sets using iteratively reweighted least squares," *Comput. Optim. Appl.*, vol. 58, no. 3, pp. 543–561, Jul. 2014. doi: [10.1007/s10589-014-9643-2](https://doi.org/10.1007/s10589-014-9643-2).



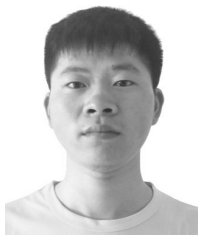
**DONGMEI WU** received the B.S. degree in computer science and the M.S. degree in automation engineering from Heilongjiang University, in 1990 and 1993, respectively, and the Ph.D. degree from the Harbin Institute of Technology, in 2003. She has been a Professor of mechatronics engineering with the State Key Laboratory of Robotics and System.



**WEIDONG WANG** received the B.S., M.S., and Ph.D. degrees in mechatronics engineering from the Harbin Institute of Technology (HIT), in 2002, 2004, and 2009, respectively. He is currently with the State Key Laboratory of Robotics and System, HIT. His research expertise is involved in the general areas of robotics and mechatronics. His research interests including motion planning, computer vision, human-machine interaction, and its application in field robot and surgical robot.



**WENRUI GAO** was born in Liaoning, China, in 1990. He received the B.S. and M.S. degrees from the Harbin Institute of Technology, China, in 2012 and 2014, respectively, where he is currently pursuing the Ph.D. degree with the State Key Laboratory of Robotics and System. His research interests include mobile manipulator, probabilistic robotics, robot vision, and machine learning.



**HONGBIAO ZHU** received the M.S. degree in vehicle engineering from the Harbin Institute of Technology, Weihai, China, in 2017, where he is currently pursuing the Ph.D. degree with the State Key Laboratory of Robotics and System. His main research interests include multiple robotic systems and environment perception.



**GUOFU HUANG** was born in 1966, China. He received the M.S. degree in radioactive geological exploration from East China Geological Institute, in 1991. He is currently with the Radiation Monitoring Technical Centre of Ministry of Environmental Protection (RMTC). His main research interests include radiation monitoring and protection mechanism.



**ZHIQIANG DU** (M'05) received the B.S. degree in mechanical engineering and the M.S. and Ph.D. degrees in mechatronics engineering from the Harbin Institute of Technology (HIT), in 1995, 1997, and 2001, respectively. He is currently with the State Key Laboratory of Robotics and System, HIT. He has been a Professor of mechatronics engineering, since 2006. His research interests include medical robots, industrial robots, and special robots.

...